Influence of oxygen ordering kinetics on Raman and optical response in $YBa_2Cu_3O_{6.4}$

A.A. Maksimov, D.A. Pronin, S.V. Zaitsev, and I.I. Tartakovskii
Institute of Solid State Physics, Russian Academy of Sciences, Chernogolovka, Moscow district, 142432, Russia

G. Blumberg,[1,2,4] M.V. Klein,[1,2] M. Karlow,[1,2] S.L. Cooper,[1,2] A.P. Paulikas,[3] and B.W. Veal[3]
[1] *NSF Science and Technology Center for Superconductivity*
[2] *Department of Physics, University of Illinois at Urbana-Champaign, Urbana, Illinois, 61801-3080*
[3] *Materials Science Division, Argonne National Laboratory, Argonne, Illinois, 60439*
[4] *Institute of Chemical Physics and Biophysics, Rävala 10, Tallinn EE0001, Estonia*
(November 8, 1995; STCS-1154)

arXiv:cond-mat/9511071v1 15 Nov 1995

Kinetics of the optical and Raman response in $YBa_2Cu_3O_{6.4}$ were studied during room temperature annealing following heat treatment. The superconducting T_c, dc resistivity, and low-energy optical conductivity recover slowly, implying a long relaxation time for the carrier density. Short relaxation times are observed for the B_{1g} Raman scattering – magnetic, continuum, and phonon – and the charge transfer band. Monte Carlo simulations suggest that these two relaxation rates are related to two length scales corresponding to local oxygen ordering (fast) and long chain and twin formation (slow).

74.25.Gz, 74.25.Ha, 78.30.Er, 61.43.Bn

Room temperature (RT) annealing has been observed in oxygen deficient $YBa_2Cu_3O_{6+x}$ single crystals rapidly quenched from elevated temperatures ($T \approx 420$ K) [1]. It is generally believed that the disorder produced by heating is frozen by the fast quench, and that RT annealing results from re-ordering of oxygen in the CuO-chain layer via diffusion. The oxygen re-ordering lowers the average valence of the chain Cu and transfers holes to the CuO_2-planes. Thus far, the influence of RT annealing has been seen experimentally in the superconducting transition temperature, T_c [1], the Raman 2-magnon line (2-ML) and electronic continuum intensity [2], and various structural [3] and optical [4] parameters. However, a detailed understanding of the kinetics involved has yet to be achieved.

We have investigated the kinetics of several physical properties of underdoped $YBa_2Cu_3O_{6.4}$ on the same sample during reproducible quench/anneal cycles, and find two characteristic behaviors. One is exhibited by the dc resistivity, T_c, and the low-frequency (LF) optical spectral weight, all of which recover slowly over a few days following heat treatment. In sharp contrast, the optical charge-transfer band (CTB), the B_{1g} Raman 2-ML, electronic continuum, and phonon intensity relax rapidly during the first hours of RT annealing. Since the dc resistivity and T_c involve the CuO_2-plane carrier density directly, our results suggest that the rapid relaxation of the second group occurs through a process that is independent of chain-to-plane charge transfer.

Monte Carlo simulations of oxygen ordering in the chains also show two relaxation rates: one fast, corresponding to short range oxygen order where the correlation length is of order the lattice constant, $r \approx a$; and one slow, where the correlation length is large compared to a. We conclude from these results that the fast relaxation processes depend on short range correlations, whereas long range oxygen order is important to the slower processes.

As shown in the inset of Fig. 1, the underdoped $YBa_2Cu_3O_{6.4}$ single crystal used for these measurements displays a sharp superconducting transition ($\Delta T_c \lesssim$ 1–1.5 K) at each quench/anneal cycle, despite T_c changes from 18 K before the thermal treatment to 2.9 K immediately following the quench. The reproducibility of these results for many cycles indicates that the total oxygen content of the sample remains constant. The homogeneity of the oxygen distribution at the 1 μm level was confirmed by micro Raman experiments.

The optical reflectance at near-normal incidence in the energy range $\omega = 0.03$–2.25 eV was measured at successive times following thermal treatment using a rapid-scan Michelson interferometer. A Kramers–Kronig transformation [5] was applied to obtain the optical conductivity $\sigma(t,\omega)$ from the measured reflectance data. Since variations in the high frequency reflectance ($3.8 < \omega < 4.3$ eV) [4] cause changes of less then 5% in the conductivity $\sigma(t,\omega)$ for $\omega < 2.5$ eV, ellipsometric data measured after complete relaxation were used in the energy range $\omega = 2.25$–6 eV to make this transformation. The inset of Fig. 2 shows $\sigma(t,\omega)$ for $YBa_2Cu_3O_{6.4}$ at two times t following the quench, $t_0 = 10$ min and t_∞ (fully relaxed). Immediately after the quench, the largest changes in $\sigma(t,\omega)$ are a decrease in the LF spectral weight (box 1 in the inset), and an increase in the CTB spectral weight (box 2) [7]. The LF spectral weight (box 1) is comprised of a Drude part due to holes in the CuO_2-planes plus a mid-IR peak associated with chain conductivity [6]. In Fig. 2 we plot as a function of time the variation in effective number of carriers (integrated spectral weight), $\Delta N_{1,2}(t) = C \int_{box\,1,2} [\sigma(t,\omega) - \sigma(t_\infty,\omega)]\, d\omega$, where the constant C is given in Eq. (3) of Ref. [7]. We find that $\Delta N_2(t)$ takes ≈ 100 min to recover to its initial value,

whereas complete recovery of $\Delta N_1(t)$ requires several days. Moreover, the sum $\Delta N(t) = \Delta N_1(t) + \Delta N_2(t)$ during the first $\sim$ 100 min remains approximately constant. These results are significant because they suggest that the transfer of spectral weight from the CTB to LF band occurs quite rapidly relative to the time scale associated with chain-to-plane charge transfer. Notably, the monotonic increase in $\Delta N_1(t)$ at long times may reflect different effective masses for holes in the chain and the plane layers.

Raman scattering (RS) data from single crystal $YBa_2Cu_3O_{6.4}$ was obtained in 20 second intervals at successive times following the quench using a CCD equipped Raman triple spectrometer. The 2-ML [8,9] and electronic continuum [9,10] spectra were obtained at room temperature, while the 336 cm^{-1} phonon scattering data were taken at 5 K. The inset of Fig. 3 presents the RS spectrum measured at $t_0 = 6$ min after the quench in the $x'y'$ (mainly B_{1g}) geometry. Fig. 3 shows the temporal dependence of the 2-ML and electronic background (0.1 to 0.5 eV) intensities. An increase of both the 2-ML and low-frequency RS background intensities is observed after quenching; however the fractional increase is larger for the background than for the 2-ML. Interestingly, the main change in the intensity for both features occurs during the initial 50–100 min, although complete recovery to pre-quench values takes several days.

At least two characteristic relaxation rates may be extracted from Figs. 1–3 if an exponential temporal dependence of the form $A(t) - A(t_\infty) = [A(t_0) - A(t_\infty)]\exp(-t/\tau)$ is assumed. In order to estimate these times, we have represented the data as

$$L_A(t) \equiv \ln\left|\frac{A(t) - A(t_\infty)}{A(t_0) - A(t_\infty)}\right|, \qquad (1)$$

where $A(t)$ is one of the measurable quantities and $A(t_0)$ is the first measured value of A just after the quenching.

Figure 4a plots $L_A(t)$ for the optical and RS quantities, and T_c. Two distinct relaxation behaviors are clearly seen. The kinetics of T_c and $\Delta N_1(t)$ demonstrate a single long relaxation time, estimated to be $\tau \approx 250$ min via a straight line least squares fit to the experimental points in the range $t = 0 - 200$ min. In [11], the kinetics of the dc resistivity and T_c during room temperature annealing were shown to be of the same order. By contrast, the kinetics of 2-ML, background intensity, the integrated intensity of the B_{1g} phonon and $\sigma(t,\omega)$ in the CTB spectral region demonstrate two relaxation times: an initially short relaxation ($\tau \approx 50$ min) over the first ≈ 100 min, followed by a considerably slower relaxation.

To gain insight into the experimental data, we carried out a Monte Carlo simulation of the oxygen distribution kinetics in the CuO-chains of $YBa_2Cu_3O_{6+x}$. We used the asymmetric next-nearest-neighbor Ising model [12], which takes into account three different effective pair interactions between oxygen atoms ($V_1 = 367$ meV, $V_2 = -0.348V_1$ and $V_3 = 0.159V_1$) [13]. This model has been used previously [13,14] for collecting snapshots of oxygen placement in the CuO-chains at each Monte Carlo step to study the kinetics of oxygen ordering, and also as a method for determining final oxygen structure [15,16]. We parameterize the results of these simulations in terms of an ordering parameter α, which measures how close the structure is to the ordered Ortho-I (OI)-phase [17]. α is defined to be zero when the structure is fully disordered and unity when the structure is in the ideal OI-phase. We calculate α for different correlation distances r by comparing, at every oxygen position, the Monte Carlo oxygen arrangement on a square of side $2r$ to the perfect OI structure. We used up to 5000 Monte Carlo steps on a 128×128 lattice at room temperature, starting with a disordered structure. To compare the calculated and experimental data we defined function $L_\alpha(t)$, for the ordering parameter α that is similar to $L_A(t)$ (Eq. 1), where t_∞ is equal to 5000 Monte Carlo steps. Fig. 4b shows the time dependence of L_α for different correlation distances r with oxygen content $x = 0.4$. It is seen that the dependence of L_α on time for different r looks like the temporal dependence of the various measured quantities. For long correlation distances L_α demonstrates slow kinetics, whereas the time dependencies of L_α for short distances ($r = 1$ – 2) demonstrate two rates: fast for the initial stage and much slower at longer times. The appearance of two relaxation rates at small r results from the fact that at the initial stage of relaxation only local ordering takes place. Consequently, many little twins (a few lattice constants in size) appear. This process is rather fast and the associated correlation lengths r are quite small. The slower kinetics correspond to motion of twin walls which results in the subduction of smaller twins by larger ones. This process is revealed at all correlation distances [17]. Similar results hold for the Ortho-II ordering parameter. As expected, calculations performed for higher values of the oxygen content show less difference between the kinetics at various correlation distances.

The long relaxation times exhibited by the dc conductivity [11], T_c and $\Delta N_1(t)$ imply that the fast kinetic behavior displayed by the CTB and the B_{1g} RS features occurs before oxygen ordering in the chains causes significant hole transfer to the CuO_2-planes. Since some rapidly annealing parameters, such as the 2-ML, are believed to have their origins in the planes, *we conclude that short range oxygen-ordering in the chains gives rise to short-length-scale changes in the planes without significantly altering the average planar carrier density.*

Comparing Fig. 4a with Fig. 4b, one can conclude that the kinetics for $\Delta N_2(t)$ and for the B_{1g} symmetry RS are determined by local oxygen ordering at nearest neighbor distances. As discussed in [7], the CTB is most probably due to a local excitation of a hole in the CuO_2-planes from Cu(2) $d_{x^2-y^2}$ to the four O(2,3) $p_{x,y}$ states that

surround a first-neighbor Cu(2) site. The rapid transfer of the integrated spectral weight from $\Delta N_2(t)$ to $\Delta N_1(t)$ suggests partial delocalization of bound carriers.

The 2-ML mainly probes short wavelength magnetic excitations from the vicinity of the magnetic Brillouin zone boundary $\mathbf{k} = (\pi/a, 0)$, which occur via photon-driven superexchange between two nearest-neighboring Cu(2) spins in the antiferromagnetic surroundings. Thus, the CTB and 2-ML both require only short range antiferromagnetic order which is affected by changes in the local carrier distribution but is independent of the average carrier number. The rather fast kinetics of the Raman B_{1g} continuum implies that it is also a local excitation, perhaps of magnetic origin, *and that it is not related directly to the average carrier number.* Phonon interaction with the continuum might explain the observed phonon line intensity kinetics through a Fano-type effect, but a detailed model needs to be formulated to understand this. By contrast, the resistivity, T_c, and the LF absorption kinetics are determined by longer distance oxygen ordering connected with the formation of ordered oxygen chains several lattice constants long. The LF band has been shown to be polarized along the chain direction [7]; thus chain fragments of a minimum length are required for this band to occur.

In summary, we have measured the kinetic behavior of the magnetic susceptibility, the B_{1g} symmetry Raman scattering (2-ML, electronic continuum and the 336 cm^{-1} phonon), and the optical conductivity (LF and CTB) of $YBa_2Cu_3O_{6.4}$ single crystals during room temperature annealing. The kinetics of the Raman features and the optical conductivity in the CTB region demonstrate fast relaxation ($\tau_f \sim 50$ min). The relaxation time for the resistivity, the LF absorption, and T_c is much larger ($\tau_s \gtrsim 220$ min), implying that there is a nearly constant average carrier number for times less than τ_f. Comparing the measured kinetics with Monte Carlo model simulations we suggest that the short-length-scale excitations are responsible for the fast processes, such as B_{1g} symmetry RS and the CTB in the optical conductivity. Longer correlations ($r > 2$) are responsible for changing the resistivity, LF optical conductivity and hence the effective carrier concentration.

The joint Russian/U.S. work was supported by NATO CRG No. 92-1239, the work at Chernogolovka by RBRF 95-02-06111a, ISF NKW000 and RSP on HTSC 93193, the work at Urbana by NSF DMR 91-20000 through STCS, and the work at Argonne by US DOE W-31-109-ENG-38.

[1] B.W. Veal *et al.*, Phys. Rev. B **42**, 6305 (1990).
[2] A.A. Maksimov *et al.*, Phys. Rev. B **49**, 15385 (1994).
[3] J.D. Jorgensen *et al.*, Physica C **167**, 571 (1990).
[4] J. Kircher *et al.* Phys. Rev. B **46**, 588 (1992).
[5] F. Stern, *Solid State Physics* (Academic, New York, 1963), Vol.15.
[6] K. Widder *et al.* Physica C **232**, 82 (1994).
[7] S.L. Cooper *et al.*, Phys. Rev. B **47**, 8233 (1993).
[8] K.B. Lyons *et al.*, Phys.Rev. B **37**, 2353 (1987); K.B. Lyons *et al.*, Phys. Rev. Lett. **60**, 732 (1988).
[9] G. Blumberg, *et al.*, Phys. Rev. B **49**, 13 295 (1994).
[10] D. Reznik *et al.*, Phys. Rev. B **48**, 7624 (1993).
[11] B.W. Veal, Chun Gu, J. of Electron Spectroscopy, **66**, 321 (1994).
[12] E. Salomons and D. de Fontaine, Phys. Rev. B **41**, 11159 (1990).
[13] H.F. Poulsen *et al.*, Phys. Rev. Lett. **66**, 465 (1991).
[14] G. Ceder, R. McCormack and D. de Fontaine, Phys. Rev. B **44**, 2377 (1991).
[15] R. McCormack, D. de Fontaine and G. Ceder, Phys. Rev. B **45**, 12976 (1992).
[16] H.F. Poulsen *et al.*, Nature Lett. **349**, 594 (1991).
[17] A.A. Maksimov, D.A. Pronin, S.V. Zaitsev and I.I. Tartakovskii, unpublished work.

FIG. 1. Temporal dependencies of T_c after the quench. *Inset*: Dependence of magnetic susceptibility χ on temperature measured at different times after the quench.

FIG. 2. Temporal dependencies after the quench of the variation in the optical conductivity integrated over the LF (open circles) and CTB (filled circles) regions. *Inset*: Optical conductivity $\sigma(t, \omega)$ before the heat treatment and 10 min after the quench. Boxes 1 and 2 show the integration regions.

FIG. 3. Temporal dependencies of the intensity of the 2-magnon Raman scattering line maximum (open circles) and the background intensity (filled circles) after the quench. The vertical axis scales are anchored to the time axis at their pre-quench values (i.e., 7.7 for background and 38.5 for 2-ML). *Inset*: Raman spectrum measured in $x'y'$ geometry at $t = 6$ min after the quench. Filled region corresponds to broad structureless electronic background.

FIG. 4. (a) - Measured values $L_A(t)$ [Eq. (1)] for parameters in Figs. 1–3. Straight lines are the results of least squares fitting of experimental data at the initial stage of aging. Crosses - T_c, $\tau \approx 340$ min; squares - $\Delta N_1(t)$, $\tau \approx 220$ min; filled circles - $\Delta N_2(t)$, $\tau \approx 59$ min; triangles - background, $\tau \approx 51$ min; open circles - 2-magnon line, $\tau \approx 36$ min.

(b) - Time dependencies of L_α for calculated parameter α in $YBa_2Cu_3O_{6.4}$ crystals for different correlation distances $1 \le r \le 6$ in units of $\sqrt{2}a$.

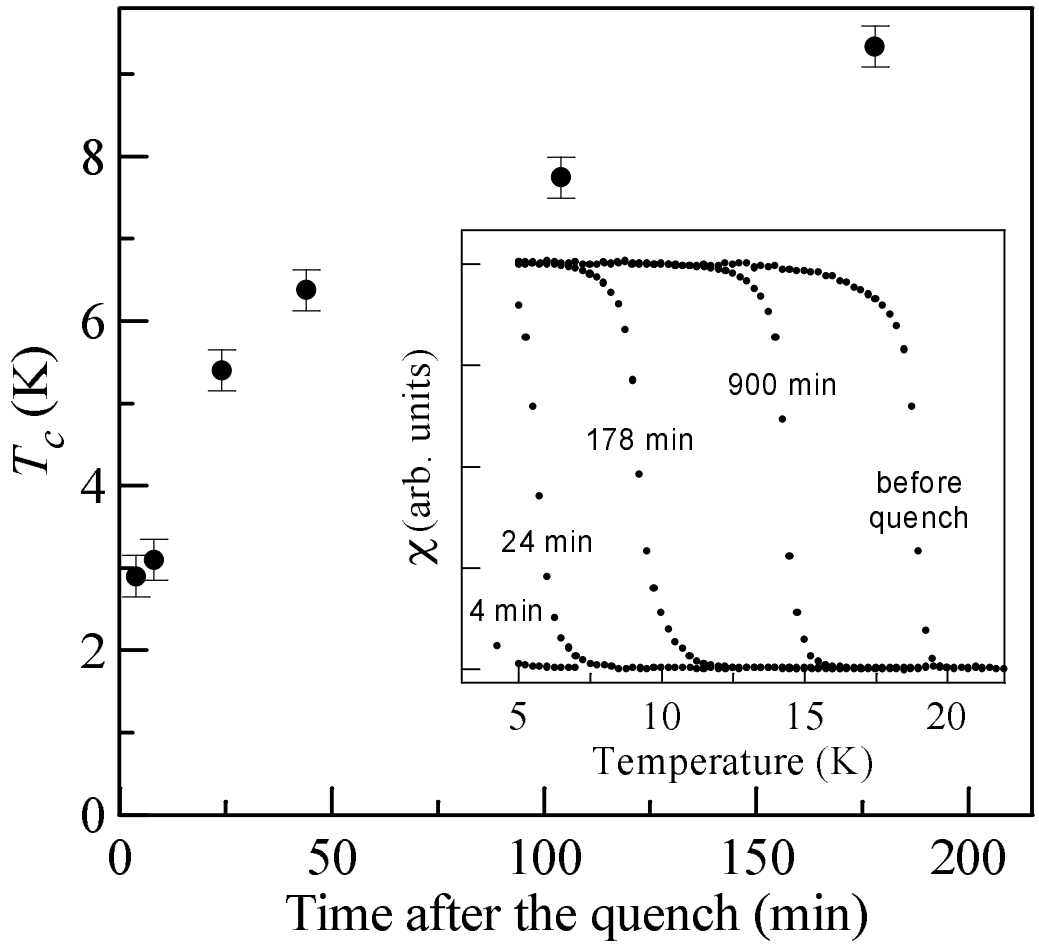
T_c (K)
0
2
4
6
8
0
50
100
150
200
Time after the quench (min)
χ (arb. units)
900 min
178 min
24 min
4 min
before quench
5
10
15
20
Temperature (K)

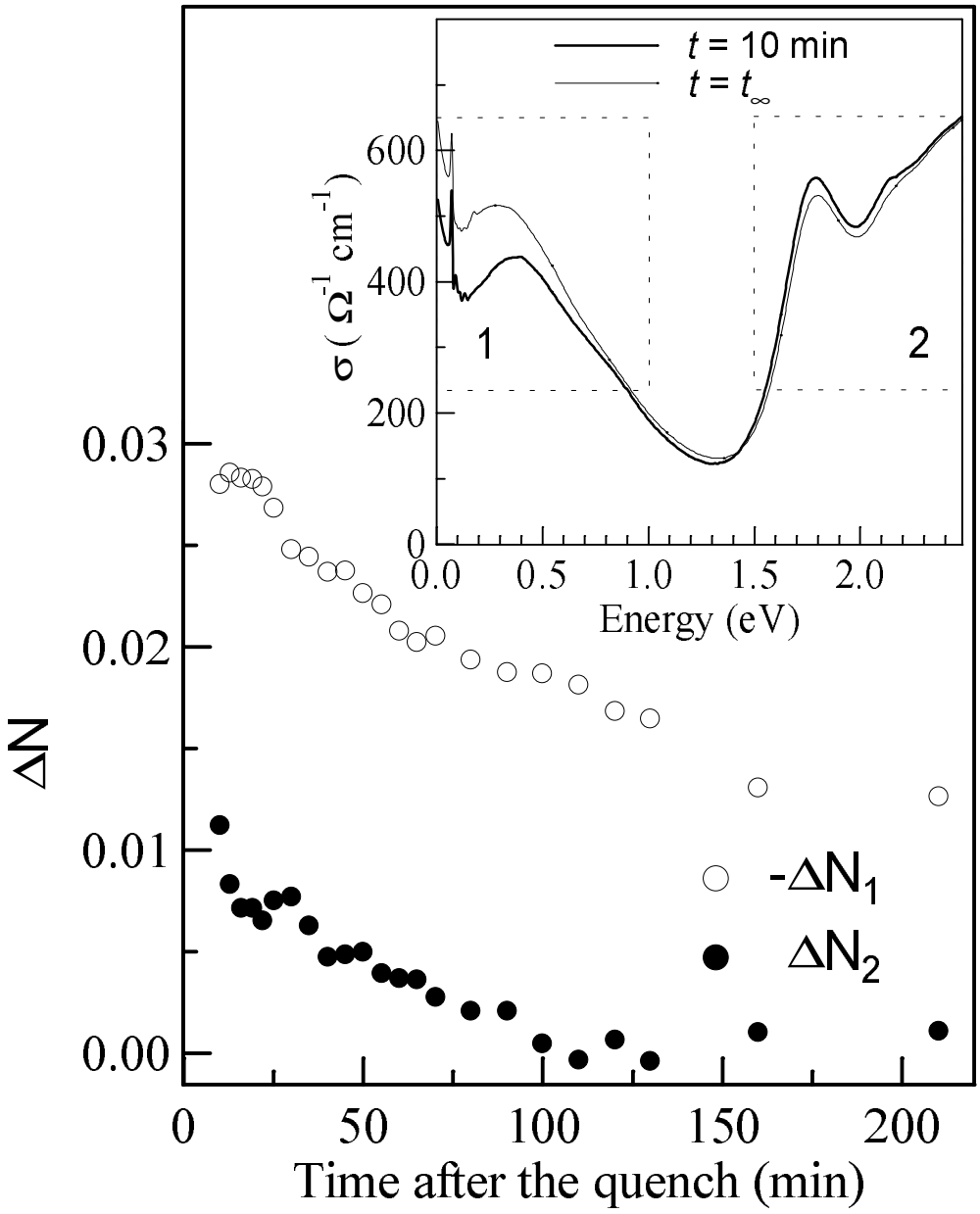
t = 10 min
t = t∞
σ (Ω-1 cm-1)
600
400
200
0
1
2
0.0
0.5
1.0
1.5
2.0
Energy (eV)
ΔN
0.03
0.02
0.01
0.00
-ΔN1
ΔN2
0
50
100
150
200
Time after the quench (min)

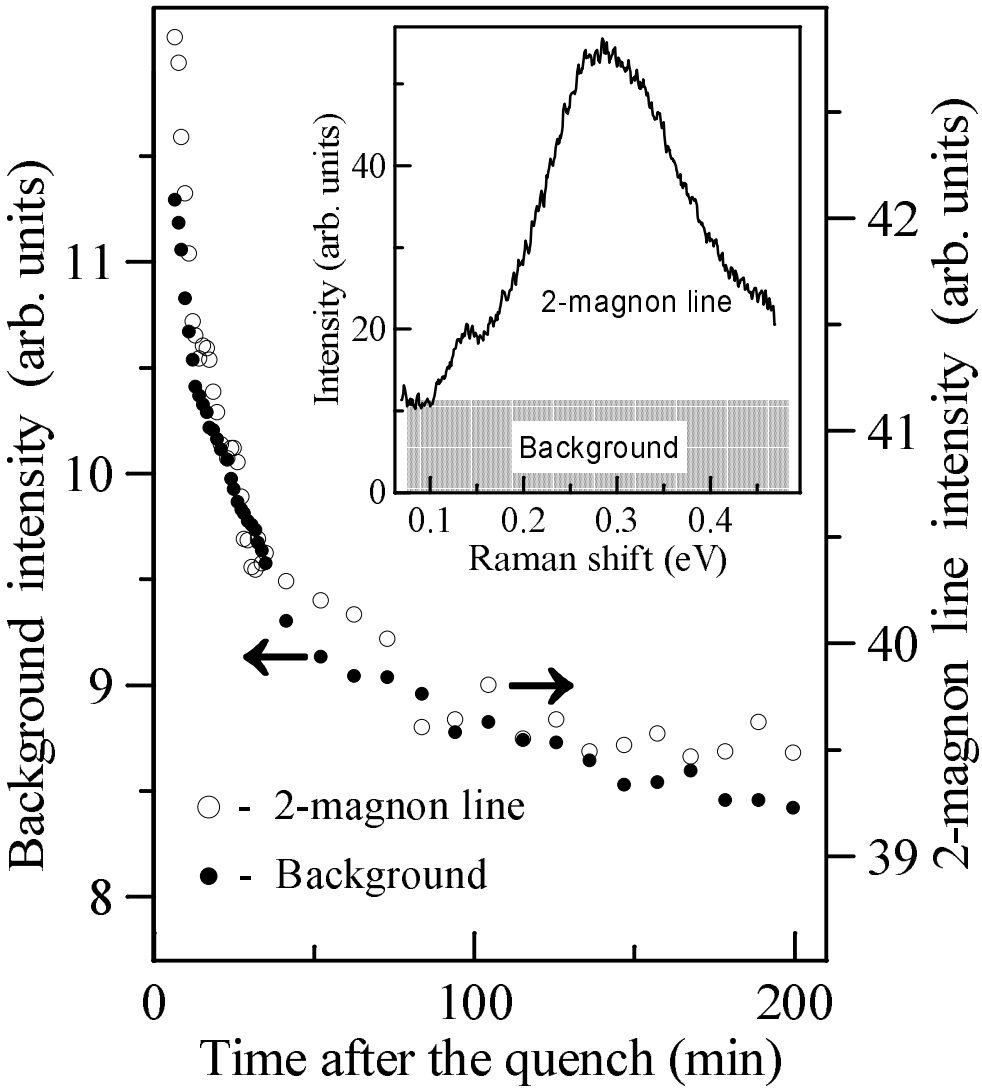
Background intensity (arb. units)
2-magnon line intensity (arb. units)
Time after the quench (min)
11
10
9
8
42
41
40
39
0
100
200
○ - 2-magnon line
● - Background
Intensity (arb. units)
40
20
0
2-magnon line
Background
0.1
0.2
0.3
0.4
Raman shift (eV)

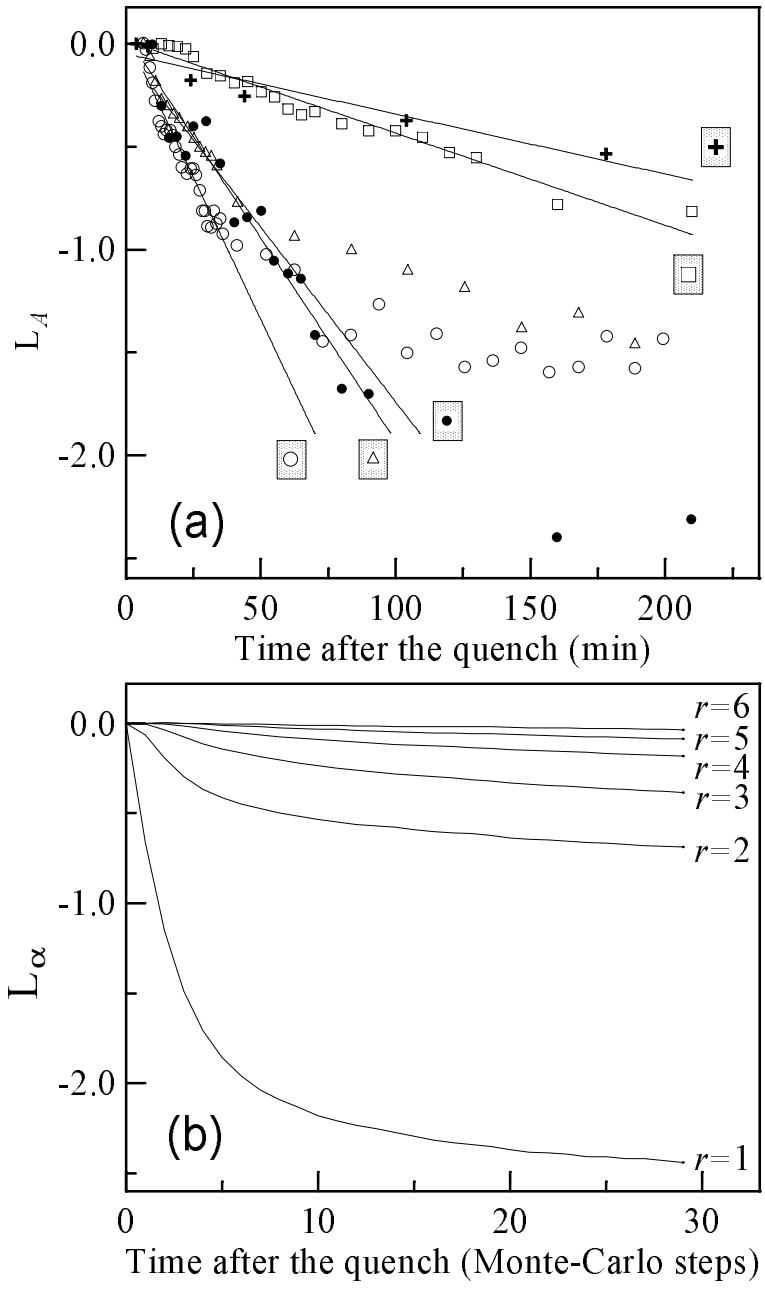
0.0
-1.0
-2.0
L_A
(a)
0
50
100
150
200
Time after the quench (min)
0.0
-1.0
-2.0
L_α
(b)
r=6
r=5
r=4
r=3
r=2
r=1
0
10
20
30
Time after the quench (Monte-Carlo steps)